https://doi.org/10.5194/acp-2022-174
Preprint. Discussion started: 29 March 2022

Atmospheric Chemistry and Physics
Discussions

Zonally Asymmetric Influences of the Quasi-Biennial Oscillation on Stratospheric Ozone

Wuke Wang[1, 2], Jin Hong[1], Ming Shangguan[3], Hongyue Wang[1], Wei Jiang[1], and Shuyun Zhao[1]

[1]Department of Atmospheric Science,China University of Geosciences,Wuhan,China
[2]Key Laboratory of Meteorological Disaster (KLME), Ministry of Education & Collaborative Innovation Center on Forecast and Evaluation of Meteorological Disasters (CIC-FEMD), Nanjing University of Information Science and Technology, Nanjing, China
[3]School of Geography and Informaiton Engineering,China University of Geosciences,Wuhan,China

Correspondence: Ming Shangguan (shanggm@cug.edu.cn)

Abstract. The Quasi-Biennial Oscillation (QBO), as the dominant mode in the equatorial stratosphere, modulates the dynamical circulation as well as the distribution of trace gases in the stratosphere. While the zonal mean changes in stratospheric ozone associated with QBO have been relatively well documented, the zonal (longitudinal) differences of the ozone signals related to QBO have been less studied. Here we demonstrate that the influences of QBO on stratospheric ozone are zonally asymmetric. Based on a composite analysis using satellite data, ERA5 reanalysis and model simulations, we found that the global distribution of stratospheric ozone varies significantly during different QBO phases. During QBO westerly (QBOW) phases, the total ozone column (TCO) and stratospheric ozone are anomalously high in the tropics, while in the mid-latitudes they are anomalously low over most of the areas, especially during the winter-spring of the respective hemisphere. This confirms the results from previous studies. In the polar region, the TCO and stratospheric ozone (50-10 hPa) anomalies are seasonal dependent and zonally asymmetric: during boreal winter (DJF), positive anomalies of TCO and stratospheric ozone are evident during QBOW over the regions from Greenland to Eurasia (60°W-120°E) in the Arctic while significant negative anomalies exist over other longitudes; in boreal autumn (SON), TCO and stratospheric ozone are anomalously high in the eastern hemisphere, but anomalously low in the western hemisphere over the Arctic; significant positive stratospheric ozone anomalies exist over the South America and Atlantic sector (60°W-60°E) of the Antarctic while negative anomalies of TCO and stratospheric ozone are seen in other longitudes during its spring (SON). The consistent features of TCO and stratospheric ozone anomalies indicate that the QBO in TCO is mainly determined by the stratospheric ozone variations. Analysis of meteorological conditions indicates that ozone anomalies associated with QBO are negatively correlated with temperature changes, suggesting that the QBO in stratospheric ozone is mainly caused by dynamical transport rather than temperature. QBO affects the geopotential height and polar vortex strength and subsequently the transport of ozone-rich air from lower latitudes to the polar region, which therefore influences the ozone concentrations over the polar regions. The geopotential height anomalies are zonally asymmetric with clear wave-1 features, which indicates that QBO influences the polar vortex and stratospheric ozone mainly by modifying the wave number 1 activities.

1 Introduction

Ozone is one of the most important trace gases in the stratosphere (Solomon, 1999; Fahey et al., 2018). The ozone layer in the stratosphere protects the life on the Earth by absorbing the Ultraviolet (UV) Radiation (Solomon, 1999; Fahey et al., 2018). Because of its strong absorption to UV radiation, ozone determines the thermal structure of the stratosphere (Son et al., 2008; Kodera et al., 2016; Fahey et al., 2018). Changes in ozone influence the temperature in the stratosphere significantly and subsequently modify the stratospheric circulation due to the thermal-dynamical balance (Son et al., 2008; Xie et al., 2016; Solomon et al., 2016; Banerjee et al., 2020). On the other hand, changes in the stratospheric circulation, in turn, may cause a redistribution of ozone in the stratosphere because of the dynamical transport (Tweedy et al., 2017; Coy et al., 2016; Wang et al., 2019). Therefore, processes like the El Niño–Southern Oscillation (ENSO) and the Quasi-Biennial Oscillation (QBO), which have important influences on the interannual variations of the stratospheric circulations, affect the stratospheric ozone significantly (e.g. Lee et al., 2010; Xie et al., 2014; Lu et al., 2019; Xie et al., 2020).

The influences of QBO, which is the dominate mode of interannual variability in the equatorial stratosphere (Baldwin et al., 2001), on ozone has been studied by lots of previous studies (e.g. Randel and Wu, 1996; Lu et al., 2019; Xie et al., 2020; Zhang et al., 2021). QBO appears as alternating easterly and westerly winds that propagate down from the top (∼50 km) to the bottom (∼16 km) of the stratosphere, with a period of about 28 months (Baldwin et al., 2001; Anstey and Shepherd, 2014; Coy et al., 2016). Such changes in zonal winds modify the vertical propagation of planetary waves and influence the strength of the polar vortex as well as the Brewer-Dobson circulation (BDC) according to the Holton-Tan mechanism (Holton and Tan, 1980, 1982; Watson and Gray, 2014; Zhang et al., 2019; Baldwin et al., 2019), and therefore play an important role in determining the dynamical circulation in the whole stratosphere (Naoe and Shibata, 2010; Garfinkel and Hartmann, 2011a, b; Anstey and Shepherd, 2014; Andrews et al., 2019; Zhang et al., 2020). Changes in stratospheric circulation during different QBO phases subsequently influence the redistribution of stratospheric compositions (Tweedy et al., 2017; Xie et al., 2020). For example, many studies have reported QBO signals in methane, water vapour and ozone (Randel and Wu, 1996; Tian et al., 2006; Lu et al., 2019; Tao et al., 2019).

QBO signals in total column ozone (TCO) have been reported over 30 years ago using observations from surface Dobson stations (Hamilton, 1989) and satellites (Bowman, 1989; Tung and Yang, 1994). During QBO westerly (QBOW) phases, TCO is anomalously high in the tropics but low in extratropics (Bowman, 1989; Hamilton, 1989; Tung and Yang, 1994). Besides such features, a seasonal synchronization, i.e., ozone anomalies are only significant during winter-spring of each respective sphere in extratropics, is also indicated. The vertical structure of QBO signals in stratospheric ozone is then investigated using satellite data (e.g. Hasebe, 1994; Randel and Wu, 1996) and model simulations (e.g. Butchart et al., 2003; Tian et al., 2006; Hansen et al., 2013). A double-peaked structure of ozone variations associated with QBO is clear in both the tropics and midlatitudes, with one peak in the lower stratosphere (20-30 km) and the other in the middle stratosphere (30-40 km). With a longer record of ozone observations as well as more other data available, studies further investigated the combined influences of QBO and other processes like ENSO on stratospheric ozone (Lee et al., 2010; Xie et al., 2014; Lu et al., 2019; Xie et al., 2020). The role of chemical processes in determining the ozone QBO is also studied (Zhang et al., 2021). So far, the impacts of QBO on TCO and stratospheric ozone have been relatively well documented. However, all the studies mentioned above are focusing on the zonal mean features. The global distribution of TCO and stratospheric ozone anomalies related to QBO has not been investigated to our understanding. While the global pattern of ozone changes is important to regional life protecting and weather and climate changes, it is interesting to look through the zonal differences of QBO in ozone.

This study investigates the global distribution (both zonal and meridional) of ozone anomalies related to QBO using satellite observations together with model simulations. Details of the data and methods used in this study are described in Section 2. Results, including the influences of the QBO on total column ozone (TCO), zonal mean ozone, ozone at different latitudes and longitudes as well as a possible mechanism are provided in Section 3. In Section 4, we give the conclusions and a discussion.

2 Data and Methods

2.1 Ozone data from Satellites

Three types of ozone products from the Copernicus Climate Change Service (C3S), including Total Column Ozone (TCO), zonal mean merged product from limb sensors and latitude-longitude gridded merged concentration product from limb sensors, are used in this study. The TCO data is from MSR2 (Multi-Sensor Reanalysis, version 2), which spans the period 1979-2020 with a horizontal resolution of $0.5° \times 0.5°$. The zonal mean product merged ozone data from limb sensors of ACE (Atmospheric Chemistry Experiment onboard SCISAT), GOMOS (Global Ozone Monitoring by Occultation of Stars onboard ENVISAT), MIPAS (Michelson Interferometer for Passive Atmospheric Sounding onboard ENVISAT), OMPS (Ozone Mapping Profiler Suite on board NPP), OSIRIS (Optical Spectrograph and InfraRed Imager System onboard ODIN), SAGE-2 (Stratospheric Aerosol and Gas Experiment II onboard ERBS) and SCIAMACHY (Scanning Imaging Absorption Spectrometer for Atmospheric Cartography on board ENVISAT). It is available from 1984 to 2020, with a meridional resolution of 10 ° and covering 41 vertical levels from 10 km to 50 km. The 3-D ozone products merged ozone data from limb sensors of GOMOS, MIPAS, OSIRIS and SCIAMACHY. This data has a horizontal resolution of $20° \times 10°$ (longitude × latitude) and a vertical resolution of 1 km from 10 km to 50 km, and is only available for the period 2002-2020. The data are accessible from the website: https://cds.climate.copernicus.eu/cdsapp#!/dataset/satellite-ozone-v1?tab=form (accessed on 16 February 2022). According to the product quality assessment done by Copernicus Climate Change Service, biases at the order of -0.13±0.11% were reported for the MSR2 TCO data, compared to the ground-based Dobson measurements (https://datastore.copernicus-climate.eu/documents/satellite-ozone/C3S_312b_Lot2.3.2.1_202002_PUGS_O3_v1.21.pdf). More details of the data can be found at https://cds.climate.copernicus.eu/cdsapp#!/dataset/satellite-ozone?tab=overview.

2.2 ERA5 reanalysis data

The ERA5 reanalysis, which is the newest generation reanalysis product produced by the ECMWF Integrated Forecast System and released in 2018, is used in this study. The original model has 137 hybrid sigma model levels from the surface to the model top at 0.01 hPa. The horizontal resolution of the model is about 31 km. ERA5 assimilates a large number types of observations, including newly reprocessed data sets, recent instruments and cell-pressure corrected SSU, improved bias correction for radiosondes, etc., into global estimates using a 4D-Var data assimilation system. Especially, ERA5 assimilated numerous satellite ozone observations, including OMI (Ozone Monitoring Instrument), SCIAMACHY, MIPAS, GOME, GOME-2 and MLS (Microwave Limb Sounder) etc. (Hersbach et al., 2020), which helps the ozone in ERA5 performs in good agreement with observations in the stratosphere (Shangguan et al., 2019). ERA5 covers a record of the global atmosphere from 1950 to the present. The ozone and other meteorological parameters in ERA5 for the period 1979-2020 are used in this study. More details about ERA5 can be found at the website:https://confluence.ecmwf.int/display/CKB/ERA5%3A+data+documentation.

2.3 Model simulations with CESM-WACCM

To confirm the QBO impacts on ozone, a pair of simulations with NCAR's CESM model (version 1.0.2) is employed in this study. The model is integrated with its fully coupled mode, with interactive ocean, land, sea ice and atmosphere processes. To better represent the stratospheric ozone, the atmospheric component of WACCM (version 4), with detailed stratospheric dynamics and chemistry is used. The model covers a vertical range from the surface to about 140 km (Marsh et al., 2013). The horizontal resolution of the model is 1.9 °× 2.5 °(latitude × longitude) for the atmosphere and approximately 1 degree for the ocean, with 66 vertical levels.

We first conducted a control run (Natural run), which includes all natural forcings like solar variability, interactive ocean, volcanic aerosols and a nudged QBO (Matthes et al., 2010). The solar and volcanic aerosol forcings are derived from observations for the period 1955-2004 and then based on future projection (2004-2099) following the SPARC (Stratospheric Processes and their Role in Climate) CCMVal (Chemistry-Climate Model Validation Activity) REF-B2 scenarios (SPARC-CCMVal, 2010). The QBO forcing time series is determined from the observed climatology of 1953-2004 via filtered spectral decomposition of that climatology. This gives a set of Fourier coefficients that can be expanded for any day and year in the past and the future. Anthropogenic forcing like greenhouse gases (GHGs) and ozone depleting substances (ODSs) are set to constant 1960s conditions to better illustrate the natural variability. In addition to the Natural run, a NOQBO run (without QBO nudging) is also employed to do a comparison. While all other configurations of the two model simulations are the same, the difference between these two simulations specifies exactly the influences of the QBO nudging.

2.4 Methods

A composite analysis based on the time series of a QBO index is used to investigate the influences of the QBO on ozone and meteorological parameters. Because of the downward propagating of easterly and westerly regimes, the phase of the QBO is different while selecting QBO indices at different levels (Anstey and Shepherd, 2014). Here we follow the method as indicated by previous studies (Wallace et al., 1993; Randel et al., 2009; Wang et al., 2015), which applied an Empirical Orthogonal Function (EOF) analysis to the equatorial zonal wind in the stratosphere (70-10 hPa). The observed equatorial zonal winds are provided by the Free University of Berlin (FUB) http://www.geo.fu-berlin.de/en/met/ag/strat/produkte/qbo/index.html. A pair of orthogonal principle components (PCs) can be obtained from this EOF analysis (Fig. 1). The first principal component (PC1) of the EOF mode is synchronized with the 20 hPa equatorial zonal wind with a correlation coefficient of 0.99, while the second

PC (PC2) is synchronized with the 50 hPa equatorial zonal wind with a correlation coefficient of 0.93. PC1 is selected as the QBO index in this study to indicate the influences of QBO on stratospheric ozone. This is due to 2 reasons: 1) PC1 is close to the middle stratosphere (10 hPa), where the ozone mixing ratios are highest; 2) The sample size of QBOW and QBOE is nearly equal to each other, while the QBOW size is usually much larger than the QBOE size using PC2 (Fig. 1). We then define the QBO westerly (PC1 > 0.5, QBOW) and easterly (PC1 < 0.5, QBOE) phases based on PC1 (Fig. 1a). The QBO associated signals can be obtained by the differences in focusing parameters during QBOW and QBOE phases (QBOW-QBOE). We also check the sensitivity of the results to the standard to define the QBO phases (e.g. using the 0 instead of 0.5 standard deviation of the QBO index) and the results persist.

As indicated by previous studies, the zonal mean ozone anomalies associated with QBO are mainly caused by the vertical transportation, which is dominated by the corresponding changes in the meridional overturning circulation in the stratosphere, i.e. the Brewer-Dobson Circulation (BDC) (Butchart, 2014; Coy et al., 2016). To explain the vertical structure of the QBO in ozone, the vertical component of the BDC in the meridional plane is calculated using the Transformed Euler Mean (TEM) equation (Andrews et al., 1987) as follows:

$$\overline{w^*} = \overline{w} + \frac{1}{acos\phi}\left(\frac{cos\phi\overline{v'\Theta'_z}}{\overline{\Theta}_z}\right)_\phi \qquad (1)$$

Where v and w are the horizontal and vertical winds, ϕ denotes the geopotential, Θ is the potential temperature, overbar and prime denote the time mean and deviation of the zonal mean, respectively.

3 Results

3.1 Influences of QBO on Total Column Ozone

We first revisit the QBO impacts on the TCO using the newest satellite-based multi-sensor reanalysis data (MSR2) with a data record over 40 years (1979-2020). From the MSR2 data, monthly anomalies of TCO near the equator (10°S-10°N) are anomalously high during QBOW phases compared with QBOE. At the same time, negative anomalies of TCO can be seen from the subtropics (15°) to mid-latitude (50°) in both hemispheres (Fig. 2a). This is consistent with the results from previous studies (Bowman, 1989; Hamilton, 1989; Tung and Yang, 1994). In addition, significant TCO anomalies are also seen in the polar regions of both hemispheres. Positive TCO anomalies are evident during QBOW over the regions from Greenland to Eurasia (60°W-120°E) in the north pole (NP) while significant negative TCO anomalies exist over other regions of the NP. Significant positive anomalies of TCO exist over the South America and Atlantic sector (60°W-60°E) of the south pole (SP) while negative TCO anomalies over other areas of the SP. This indicates zonally asymmetric features of TCO anomalies related to the QBO, which has not been reported by previous literature to our understanding. Such QBO features are very similar in ERA5 (Fig. 2b) to that seen in MSR2, indicating that ERA5 has a very good representation of the TCO variations. The Natural simulation by the CESM-WACCM model represents the TCO anomalies associated with the QBO pretty well. The spatial pattern of TCO anomalies associated with QBO from the WACCM simulation as seen in Fig. 2c shows very good consistency with that from the MSR2 data (Fig. 2a) in most of the areas, except that TCO anomalies in the SP are all positive. The magnitude of the negative anomalies in the subtropics from the CESM-WACCM model simulation is also slightly larger than that from the MSR2 and ERA5. Without the QBO nudging, the TCO signals related to QBO disappear in the NOQBO run. While the only difference between the two model simulations is the QBO nudging, this result indicates that the method of the composite analysis used in this study and the QBO related features mentioned above are robust.

As mentioned in previous studies, there is a seasonal synchronization in QBO related TCO signals (Hamilton, 1989; Tung and Yang, 1994). TCO anomalies are only significant during the winter-spring of each respective sphere in extratropics. We therefore checked the QBO in TCO during 4 different seasons based on the QBO index in each season (an example of the QBO index in boreal winter is shown in Fig. S1). Fig. 3 gives the global distribution of the TCO anomalies in different seasons resulting from a composite analysis using the MSR2 data. In all 4 seasons, positive TCO anomalies are seen near the Equator. This is consistent with previous studies, which indicated that the TCO signals in the tropics are not seasonal dependent (Bowman, 1989). Also consistent with earlier results, the negative TCO anomalies are more significant during the winter-spring of each respective sphere in extratropics. However, some new features are found in our analysis in the global distribution: the TCO QBO in NP winter is zonally asymmetric, with positive anomalies over the regions from Greenland to Eurasia (60°W-120°E) and negative anomalies over other regions; some TCO signals are also significant during boreal autumn in the northern hemisphere (NH) with zonally asymmetric features, i.e. positive TCO anomalies over Eurasia and negative TCO anomalies over the North American Arctic.

3.2 Vertical Structure of the Influences of QBO on Stratospheric Ozone

The latitude-pressure cross-sections of ozone monthly anomalies associated with QBO from different data are shown in Fig. 4. From the merged satellite data, there are double-peaks of positive ozone anomalies over the equator during QBOW phases, which is consistent with previous studies (Randel and Wu, 1996; Xie et al., 2020; Zhang et al., 2021). In the extratropics (from subtropics to midlatitudes), there are also double-peaks features of the negative ozone anomalies associated with QBO, with one peak in the lower stratosphere (70-30 hPa) and the other in the middle stratosphere (20-5 hPa). QBO signals in ERA5 ozone (Fig. 4b) are in good agreement with the merged satellite data. The CESM-WACCM model also shows good consistency with the satellite and ERA5 data in the Natural run with a QBO nudging (Fig. 4c), although the negative signals are extended higher up to the upper stratosphere in the extratropics. Without a QBO nudging, the signals are all blank indicating the robust contribution of the QBO nudging to the ozone signals in the stratosphere Fig. 4d.

The vertical structure of QBO in stratospheric ozone in different seasons is sown in Fig. 5. Similar to the TCO signals, the equatorial ozone signals related to QBO are seasonal independent with positive ozone anomalies in the lower and middle stratosphere in all seasons. The QBO signals in ozone are mainly significant during the winter-spring of each respective sphere in extratropics. Note that there are some positive ozone anomalies during the QBOW phases in the SP during JJA. To understand the reason for the vertical structure of ozone anomalies associated with QBO, the corresponding changes in the vertical component of the BDC are presented in Fig. 6. Seen from the climatological distribution, ozone volume mixing ratio peaks in the tropics in the middle stratosphere at 10 hPa (Fig. S2). During QBOW phase, the vertical component of the BDC (w*) in the tropics is anomalously weak in the lower stratosphere and strong in the middle stratosphere in all seasons (Fig. 6), which transports ozone-poor air from the troposphere to the lower stratosphere and ozone-rich air from the mid stratosphere to upper levels and therefore leads to negative ozone anomalies in the lower stratosphere and positive ozone anomalies between 15 to 3 hPa (Fig. 5). Significant negative anomalies of w* can be seen in the subtropics and midlatitudes, especially during winter of each respective sphere (Fig. 6), which means enhanced downward motion in these regions bringing ozone-poor air from upper levels to the middle and lower stratosphere.

3.3 Global distribution of QBO Signals in Stratospheric Ozone

We now discuss the global effects (both meridional and zonal) of the QBO on stratospheric ozone, which have not been documented before. Fig. 7 shows the global distribution of monthly ozone anomalies related to QBO at ∼10 hPa by a composite analysis using different data sets. From the merged satellite data, the spatial pattern of the ozone QBO is similar to that seen in the TCO anomalies as shown in Fig. 2. During the QBOW phase, positive ozone anomalies are evident near the equator while negative ozone anomalies are significant from the subtropics to midlatitudes. Zonally asymmetric features are also seen in the polar regions of both hemispheres (Fig. 7a). The ERA5 data again show a consistency with the satellite data except that the zonally asymmetric feature in the SP is not that obvious (Fig. 7b). The CESM-WACCM model, however, shows some differences with the satellite, with few signals in the tropics. This is due to the shift of the ozone QBO to slightly higher altitudes as shown in Fig. 4c. Without a QBO nudging, the QBO signals seen in Fig. 7c disappear (Fig. 7d), indicating again a robust influence of the QBO on stratospheric ozone.

Fig. 8 gives the global distribution of stratospheric ozone anomalies (at 10 hPa) related to QBO in different seasons using the merged satellite data. Again, the signals are all positive in 4 seasons during QBOW near the equator. Negative ozone anomalies are significant during the winter-spring of the respective hemisphere from the subtropics to the midlatitudes. These features are similar to the TCO anomalies shown in Fig. 3, indicating that the changes of ozone in the middle stratosphere play a dominant role in the TCO changes. The zonally asymmetric features in the polar regions during boreal winter in the NP and boreal autumn in both hemispheres are more evident. Especially, clear and significant zonally asymmetric ozone anomalies in both the Arctic and Antarctic regions can be seen in boreal autumn (SON), which have not been documented in previous literature to our understanding. In the Arctic, positive anomalies are seen in the eastern hemisphere while negative anomalies can be found in the western hemisphere. In the Antarctic, positive anomalies are mainly located in the Atlantic sector while negative anomalies are more evident in the eastern hemisphere. It is also interesting that there are some positive ozone anomalies over the Antarctic during its winter, which was not mentioned by other studies. However, such positive ozone anomalies are very weak and not significant from the ERA5 data (Fig. S3), indicating that there are large uncertainties in these positive anomalies over the Antarctic. With a longer period of data (1979-2020), ozone anomalies over the Arctic during its winter are more significant in the ERA5 data compared to the satellite data. Similar QBO signals in ozone can be found in the lower stratosphere (Fig. S4), indicating that ozone changes in both the lower stratosphere and the middle stratosphere contribute to the QBO in TCO, which is consistent with previous studies (Randel and Wu, 1996).

3.4 Dynamical Mechanism

As introduced in the Introduction, stratospheric ozone is related to complex photochemical processes which are temperature-dependent as well as dynamical transport. The meteorological conditions are therefore important for stratospheric ozone variations. To understand the possible mechanism of QBO impacts on stratospheric ozone, meteorological parameters from the ERA5 reanalysis are analyzed. Fig. 9 shows the global distribution of zonal wind (U) anomalies (shading) associated with QBO and the climatological U (contour lines) in the middle stratosphere (at 10 hPa). While there are westerly anomalies in the tropics during QBOW, asymmetric wind anomalies are seen during winter of respective hemispheres in extratropics. Easterly anomalies only exist over the Atlantic and the Mediterranean in the midlatitudes and over the north Pacific sector in the Arctic, while westerly anomalies are seen in other regions during boreal winter in the NH. In the SH, westerly anomalies can be seen over the western hemisphere of Antarctic, while easterly anomalies exist over the eastern hemisphere during its winter-spring. The results are different with previous studies (e.g. Anstey and Shepherd, 2014; Watson and Gray, 2014; Andrews et al., 2019), which indicate a strengthening of the polar vortex during winter. This is because of the different QBO index used in this study (PC1, indicating U at 20 hPa) compared to other studies (usually U at 50 hPa).

The temperature (T) anomalies at 10 hPa associated with QBO are given in Fig. 10. During QBOW phases, cold temperature anomalies are seen near the equator in all seasons. This is caused by the anomalously strong upwelling of the BDC in the tropics as seen in Fig. 6 and subsequent dynamical cooling. In the subtropics, warm temperature anomalies are dominant according to the enhanced downwelling of the BDC and subsequent dynamical warming. In the polar regions, cold anomalies are evident due to the weakening of the downwelling (Fig. 6) and subsequent less dynamical warming. Since the photochemical reactions related to ozone production are mostly temperature dependent, temperature anomalies may contribute to the ozone signals related to QBO. However, changes in temperature and ozone are opposite in sign in almost all the areas. This indicates that the ozone anomalies are mainly caused by dynamical transport rather than temperature-dependent chemical reactions.

Fig. 11 shows the geopotential height (Z) anomalies at 10 hPa during QBOW phases by a composite analysis. The geopotential height anomalies associated with QBO are less significant in the tropics with weak positive anomalies in all seasons. Zonally asymmetric Z anomalies are evident and significant in extratropics. During boreal winter (DJF), positive anomalies are evident in QBOW from eastern North America to western Eurasia over the Arctic, indicating a weaker and more disturbed polar vortex. This allows more ozone-rich air transported from lower latitudes to the polar region and leads to positive ozone anomalies in this region (Fig. 8d). Over other regions of the Arctic, there are negative geopotential height anomalies and subsequently negative ozone anomalies. During boreal summer (JJA, winter in the SH), there are also evident zonally asymmetric anomalies with QBO in geopotential height, with positive anomalies in the western hemisphere and negative anomalies in the eastern hemisphere over the Antarctic. However, ozone anomalies are all positive over the Antarctic from the merged satellite data. On the other hand, there are negative ozone anomalies in the eastern hemisphere over the Antarctic from the ERA5 data Fig. S3, although the signals are not statistically significant. Whether the ozone QBO signals over the Antarctic are zonally asymmetric awaits further investigations. In boreal autumn (SON), zonally asymmetric geopotential height anomalies are evident in both hemispheres. Positive Z anomalies are significant mainly in the eastern hemisphere over the Arctic during QBOW, while negative anomalies are evident mainly in the western hemisphere over the Arctic. Over the Antarctic, geopotential height signals change in sign with negative anomalies from 60 °W to 180 °E and positive anomalies in other regions. Such changes of geopotential height associated with QBO resemble to the pattern of ozone anomalies, indicating the important role of the strength of polar vortex in determining ozone concentrations.

To further illustrate the processes related to the geopotential height anomalies associated with QBO, we separate the monthly geopotential height anomalies into different wave numbers. Fig. 12 gives the overall changes of geopotential height as well as the corresponding changes in wave numbers 1-3 during QBOW over the NH in boreal winter (DJF). The climatological mean of the geopotential height and its wave numbers 1-3 components are also shown. Compare the signals in Fig. 12a and other figure panels, it is obvious that the geopotential height anomalies are dominated by the wave number 1 process. The QBO related wave-1 anomalies are generally out of phase with the climatological pattern with a slight eastward shift (Fig. 12b), indicating a negative interference to wave-1 activities. For wave numbers 2-3, the QBO related anomalies are much weaker compared to wave-1 and out of phase with the climatological pattern (Figs. 12c-d). In boreal autumn, the QBO anomalies in geopotential height are also dominated by the wave-1 process, and the wave-1 anomalies are out of phase with the climatological pattern (Fig. S5). For the SH in its spring (SON), the geopotential height anomalies associated with QBO are also dominated by the wave-1 process, but the wave-1 anomalies are shifted by about 90°compared to the climatological pattern (Fig. S6). The phase shift or out of phase of wave activities compared to their climatological structure is a very complex issue and is out of the scope of this study. Anyway, it is clear that the QBO affects the polar vortex mainly through wave-1 process and leads to zonally asymmetric features in geopotential height and ozone anomalies.

4 Conclusions and Discussion

The influences of the QBO on ozone have been studied for over 30 years. Here, we first revisited the influences of the QBO on TCO and zonal mean stratospheric ozone using a longer record of merged satellite data (1979-2020 for TCO and 1984-2020 for zonal mean ozone), together with the most recent ERA5 reanalysis and NCAR's CESM-WACCM model simulations. We found seasonal independent positive ozone anomalies in the tropics and negative ozone anomalies during winter-spring of the respective hemisphere in extratropics, which confirms the results from previous studies (Bowman, 1989; Hamilton, 1989; Tung and Yang, 1994; Randel and Wu, 1996; Butchart et al., 2003). The ERA5 data and the CESM-WACCM model capture the QBO in ozone very well, and a single-factor controlling simulation without QBO nudging further confirms the robustness of the QBO impacts on ozone. Some new features in TCO corresponding to QBO are also found from the global distribution pattern: zonally asymmetric TCO anomalies are evident during autumn-winter in the NH and during spring in the SH over the polar regions; positive TCO anomalies are seen from Greenland to eastern Eurasia (60°W-60°E) over the Arctic in winter (DJF) and mainly in the eastern hemisphere over the Arctic in autumn (SON); Some positive signals in TCO exist during its spring (SON) in the Atlantic sector over the Antarctic. The TCO anomalies are contributed both by the ozone changes in the lower and middle stratosphere, which are mainly caused by the vertical transport related to the vertical gradient of climatological ozone distribution and changes in the vertical component of the BDC.

We then further investigated the global distribution of ozone anomalies related to QBO in the stratosphere in monthly mean anomalies as well as in different seasons. Similar to the TCO anomalies described above, evident zonally asymmetric features can be found in ozone anomalies in the middle stratosphere associated with QBO, which are especially significant during autumn-winter (SON-DJF) over the Arctic and during spring (SON) over the Antarctic. The zonally asymmetric features of ozone in the middle stratosphere (at 10 hPa) are in general consistent with the spatial pattern of TCO as described above, indicating the dominate contribution of the stratospheric ozone to the TCO variations. According to the analysis of meteorological parameters, we found that the QBO influences on ozone are mainly related to dynamical transport rather than temperature-dependent chemical production. Besides the well-known weakening/strengthening of the polar vortex during the easterly/westerly phase of the QBO (using 50 hPa U) (Anstey and Shepherd, 2014; Watson and Gray, 2014; Andrews et al., 2019; Xie et al., 2020), QBO (using PC1 as introduced in Methods) leads to a wave-1 pattern in geopotential height anomalies over the polar regions. The wave-1 anomalies are in general out of phase with the climatological wave-1 pattern during autumn-winter in the NH but shift by 90°during spring (SON) in the SH.

Stratospheric ozone is not only essential in protecting life on the Earth, but also has important climate impacts on the surface. More and more studies reported the important role of ozone variations in modifying the stratospheric circulation and therefore influencing the surface climate (e.g. Xie et al., 2020). Since the QBO has relatively high predictability, considering its impacts on stratospheric ozone and subsequent atmospheric circulations may be helpful to improve the prediction of surface weather and climate.

Data availability. The MSR2, merged satellite data and the ERA5 reanalysis can be downloaded from the Copernicus Climate Change Service website https://cds.climate.copernicus.eu/cdsapp#!/home. The model simulations can be provided to readers by contacting the corresponding author.

Author contributions. W. W. performed the data analysis, plotted the figures and wrote the first draft of the paper. J. H., M. S., H. W. and S. Z. contributed to the interpretation of the results and revised the manuscript. W. J. contributed to the wave number analysis. All authors reviewed the manuscript.

Competing interests. The authors declare that they have no conflict of interest.

Acknowledgements. This work was supported by the Ministry of Science and Technology of the People's Republic of China (2019YFE0125000), National Natural Science Foundation of China (Grant No. 41705023 and 41875095) and the open project (KLME202003) from the Key Laboratory of Meteorological Disaster (KLME), Ministry of Education & Collaborative Innovation Center on Forecast and Evaluation of Meteorological Disasters(CIC-FEMD). We thank the Copernicus Climate Change Service for providing the satellite data, ECMWF for the ERA5 data and NCAR for the CESM-WACCM Model. The model simulations were carried out at the Deutsche Klimarechenzentrum (DKRZ) in Hamburg, by Prof. Katja Matthes’s group at the Helmholtz Centre for Ocean Research Kiel (GEOMAR), Germany.

References

Andrews, D. G., Holton, J. R., and Leovy, C. B.: Middle atmosphere dynamics, vol. 40, Academic press, 1987.

Andrews, M. B., Knight, J. R., Scaife, A. A., Lu, Y., Wu, T., Gray, L. J., and Schenzinger, V.: Observed and Simulated Teleconnections Between the Stratospheric Quasi-Biennial Oscillation and Northern Hemisphere Winter Atmospheric Circulation, J. Geophys. Res., 124, 1219–1232, https://doi.org/10.1029/2018JD029368, 2019.

Anstey, J. A. and Shepherd, T. G.: High-latitude influence of the quasi-biennial oscillation, Quart. J. Roy. Meteor. Soc., 140, 1–21, https://doi.org/10.1002/qj.2132, 2014.

Baldwin, M., Gray, L., Dunkerton, T., Hamilton, K., Haynes, P., Randel, W., Holton, J., Alexander, M., Hirota, I., Horinouchi, T., et al.: The quasi-biennial oscillation, Rev. Geophys., 39, 179–229, 2001.

Baldwin, M. P., Birner, T., Brasseur, G., Burrows, J., Butchart, N., Garcia, R., Geller, M., Gray, L., Hamilton, K., Harnik, N., et al.: 100 years of progress in understanding the stratosphere and mesosphere, Meteorological Monographs, 59, 27–1, https://doi.org/10.1175/AMSMONOGRAPHS-D-19-0003.1, 2019.

Banerjee, A., Fyfe, J. C., Polvani, L. M., Waugh, D., and Chang, K.-L.: A pause in Southern Hemisphere circulation trends due to the Montreal Protocol, Nature, 579, 544–548, 2020.

Bowman, K.: Global patterns of the quasi-biennial oscillation in total ozone, J. Atmos. Sci., 46, 3328–3343, https://doi.org/10.1175/1520-0469(1989)046<3328:GPOTQB>2.0.CO;2, 1989.

Butchart, N.: The Brewer-Dobson circulation, 52, 157–184, https://doi.org/10.1002/2013RG000448, 2014.

Butchart, N., Scaife, A., Austin, J., Hare, S., and Knight, J.: Quasi-biennial oscillation in ozone in a coupled chemistry-climate model, J. Geophys. Res., 108, https://doi.org/10.1029/2002JD003004, 2003.

Coy, L., Wargan, K., Molod, A. M., McCarty, W. R., and Pawson, S.: Structure and dynamics of the quasi-biennial oscillation in MERRA-2, J. Climate, 29, 5339–5354, 2016.

Fahey, D., Newman, P. A., Pyle, J. A., Safari, B., Chipperfield, M. P., Karoly, D., Kinnison, D. E., Ko, M., Santee, M., and Doherty, S. J.: Scientific Assessment of Ozone Depletion: 2018, Global Ozone Research and Monitoring Project-Report No. 58, WMO (World Meteorological Organization), 2018.

Garfinkel, C. I. and Hartmann, D. L.: The influence of the quasi-biennial oscillation on the troposphere in winter in a hierarchy of models. Part I: Simplified dry GCMs, J. Atmos. Sci., 68, 1273–1289, 2011a.

Garfinkel, C. I. and Hartmann, D. L.: The influence of the quasi-biennial oscillation on the troposphere in winter in a hierarchy of models. Part II: Perpetual winter WACCM runs, J. Atmos. Sci., 68, 2026–2041, 2011b.

Hamilton, K.: Interhemispheric asymmetry and annual synchronization of the ozone quasi-biennial oscillation, J. Atmos. Sci., 46, 1019–1025, https://doi.org/10.1175/1520-0469(1989)046<1019:IAAASO>2.0.CO;2, 1989.

Hansen, F., Matthes, K., and Gray, L. J.: Sensitivity of stratospheric dynamics and chemistry to QBO nudging width in the chemistry-climate model WACCM, J. Geophys. Res., 118, 10 464–10 474, https://doi.org/10.1002/jgrd.50812, 2013.

Hasebe, F.: Quasi-biennial oscillations of ozone and diabatic circulation in the equatorial stratosphere, J. Atmos. Sci., 51, 729–745, https://doi.org/10.1175/1520-0469(1994)051<0729:QBOOOA>2.0.CO;2, 1994.

Hersbach, H., Bell, B., Berrisford, P., Hirahara, S., Horányi, A., Muñoz-Sabater, J., Nicolas, J., Peubey, C., Radu, R., Schepers, D., et al.: The ERA5 global reanalysis, Quart. J. Roy. Meteor. Soc., 146, 1999–2049, 2020.

Holton, J. R. and Tan, H.-C.: The influence of the equatorial quasi-biennial oscillation on the global circulation at 50 mb, J. Atmos. Sci., 37, 2200–2208, 1980.

Holton, J. R. and Tan, H.-C.: The quasi-biennial oscillation in the Northern Hemisphere lower stratosphere, J. Meteor. Soc. Japan., 60, 140–148, 1982.

Kodera, K., Thieblemont, R., Yukimoto, S., and Matthes, K.: How can we understand the global distribution of the solar cycle signal on the Earth's surface?, Atmos. Chem. Phys., 16, 12 925–12 944, https://doi.org/10.5194/acp-16-12925-2016, 2016.

Lee, S., Shelow, D. M., Thompson, A. M., and Miller, S. K.: QBO and ENSO variability in temperature and ozone from SHADOZ, 1998-2005, J. Geophys. Res., 115, https://doi.org/10.1029/2009JD013320, 2010.

Lu, J., Xie, F., Tian, W., Li, J., Feng, W., Chipperfield, M., Zhang, J., and Ma, X.: Interannual variations in lower stratospheric ozone during the period 1984–2016, J. Geophys. Res., 124, 8225–8241, 2019.

Marsh, D. R., Mills, M. J., Kinnison, D. E., Lamarque, J.-F., Calvo, N., and Polvani, L. M.: Climate change from 1850 to 2005 simulated in CESM1 (WACCM), J. Climate, 26, 7372–7391, https://doi.org/10.1175/JCLI-D-12-00558.1, 2013.

Matthes, K., Marsh, D. R., Garcia, R. R., Kinnison, D. E., Sassi, F., and Walters, S.: Role of the QBO in modulating the influence of the 11 year solar cycle on the atmosphere using constant forcings, J. Geophys. Res., 115, 18 110, https://doi.org/10.1029/2009JD013020, 2010.

Naoe, H. and Shibata, K.: Equatorial quasi-biennial oscillation influence on northern winter extratropical circulation, J. Geophys. Res., 115, https://doi.org/10.1029/2009JD012952, 2010.

Randel, W. J. and Wu, F.: Isolation of the ozone QBO in SAGE II data by singular-value decomposition, J. Atmos. Sci., 53, 2546–2559, 1996.

Randel, W. J., Shine, K. P., Austin, J., Barnett, J., Claud, C., Gillett, N. P., Keckhut, P., Langematz, U., Lin, R., Long, C., Mears, C., Miller, A., Nash, J., Seidel, D. J., Thompson, D. W. J., Wu, F., and Yoden, S.: An update of observed stratospheric temperature trends, J. Geophys. Res., 114, https://doi.org/10.1029/2008JD010421, 2009.

Shangguan, M., Wang, W., and Jin, S.: Variability of temperature and ozone in the upper troposphere and lower stratosphere from multi-satellite observations and reanalysis data, Atmos. Chem. Phys., 19, 6659–6679, https://doi.org/10.5194/acp-19-6659-2019, 2019.

Solomon, S.: Stratospheric ozone depletion: A review of concepts and history, Rev. Geophys., 37, 275–316, 1999.

Solomon, S., Ivy, D. J., Kinnison, D., Mills, M. J., Neely, R. R., and Schmidt, A.: Emergence of healing in the Antarctic ozone layer, Science, 353, 269–274, 2016.

Son, S.-W., Polvani, L., Waugh, D., Akiyoshi, H., Garcia, R., Kinnison, D., Pawson, S., Rozanov, E., Shepherd, T., and Shibata, K.: The impact of stratospheric ozone recovery on the Southern Hemisphere westerly jet, Science, 320, 1486–1489, 2008.

SPARC-CCMVal: SPARC Report on the Evaluation of Chemistry-Climate Models, SPARC Report 5, WCRP-132, WMO/TD–1526, 2010.

Tao, M., Konopka, P., Ploeger, F., Yan, X., Wright, J. S., Diallo, M., Fueglistaler, S., and Riese, M.: Multitimescale variations in modeled stratospheric water vapor derived from three modern reanalysis products, Atmos. Chem. Phys., 19, 6509–6534, https://doi.org/10.5194/acp-19-6509-2019, 2019.

Tian, W., Chipperfield, M. P., Gray, L. J., and Zawodny, J. M.: Quasi-biennial oscillation and tracer distributions in a coupled chemistry-climate model, J. Geophys. Res., 111, https://doi.org/10.1029/2005JD006871, 2006.

Tung, K. and Yang, H.: Global QBO in circulation and ozone. Part I: Reexamination of observational evidence, J. Atmos. Sci., 51, 2699–2707, https://doi.org/10.1175/1520-0469(1994)051<2699:GQICAO>2.0.CO;2, 1994.

Tweedy, O. V., Kramarova, N. A., Strahan, S. E., Newman, P. A., Coy, L., Randel, W. J., Park, M., Waugh, D. W., and Frith, S. M.: Response of trace gases to the disrupted 2015-2016 quasi-biennial oscillation., Atmos. Chem. Phys., 17, 2017.

Wallace, J., PANETTA, R., and ESTBERG, J.: Representation of the equatorial stratospheric quasi-biennial oscillation in EOF phase space, J. Atmos. Sci., 50, 1751–1762, https://doi.org/10.1175/1520-0469(1993)050<1751:ROTESQ>2.0.CO;2, 1993.

Wang, W., Matthes, K., Tian, W., Park, W., Shangguan, M., and Ding, A.: Solar impacts on decadal variability of tropopause temperature and lower stratospheric (LS) water vapour: a mechanism through ocean–atmosphere coupling, Climate Dynamics, 52, 5585–5604, 2019.

Wang, W., Matthes, K., and Schmidt, T.: Quantifying contributions to the recent temperature variability in the tropical tropopause layer, Atmos. Chem. Phys., 15, 5815–5826, https://doi.org/10.5194/acp-15-5815-2015, 2015.

Watson, P. A. G. and Gray, L. J.: How Does the Quasi-Biennial Oscillation Affect the Stratospheric Polar Vortex?, J. Atmos. Sci., 71, 391–409, https://doi.org/10.1175/JAS-D-13-096.1, 2014.

Xie, F., Li, J., Tian, W., Fu, Q., Jin, F.-F., Hu, Y., Zhang, J., Wang, W., Sun, C., Feng, J., et al.: A connection from Arctic stratospheric ozone to El Niño-Southern oscillation, Environ. Res. Lett., 11, 124 026, 2016.

Xie, F., Zhang, J., Li, X., Li, J., Wang, T., and Xu, M.: Independent and joint influences of eastern Pacific El Niño–southern oscillation and quasi biennial oscillation on Northern Hemispheric stratospheric ozone, Int. J. Climatol., 2020.

Xie, F., Li, J., Tian, W., Zhang, J., and Sun, C.: The relative impacts of El Nino Modoki, canonical El Nino, and QBO on tropical ozone changes since the 1980s, Environ. Res. Lett., 9, https://doi.org/10.1088/1748-9326/9/6/064020, 2014.

Zhang, J., Xie, F., Ma, Z., Zhang, C., Xu, M., Wang, T., and Zhang, R.: Seasonal Evolution of the Quasi-biennial Oscillation Impact on the Northern Hemisphere Polar Vortex in Winter, J. Geophys. Res., 124, 12 568–12 586, https://doi.org/10.1029/2019JD030966, 2019.

Zhang, J., Zhang, C., Zhang, K., Xu, M., Duan, J., Chipperfield, M. P., Feng, W., Zhao, S., and Xie, F.: The role of chemical processes in the quasi-biennial oscillation (QBO) signal in stratospheric ozone, Atmos. Environ., 244, https://doi.org/10.1016/j.atmosenv.2020.117906, 2021.

Zhang, R., Tian, W., and Wang, T.: Role of the quasi-biennial oscillation in the downward extension of stratospheric northern annular mode anomalies, 55, 595–612, 2020.

(a) EOF PC1

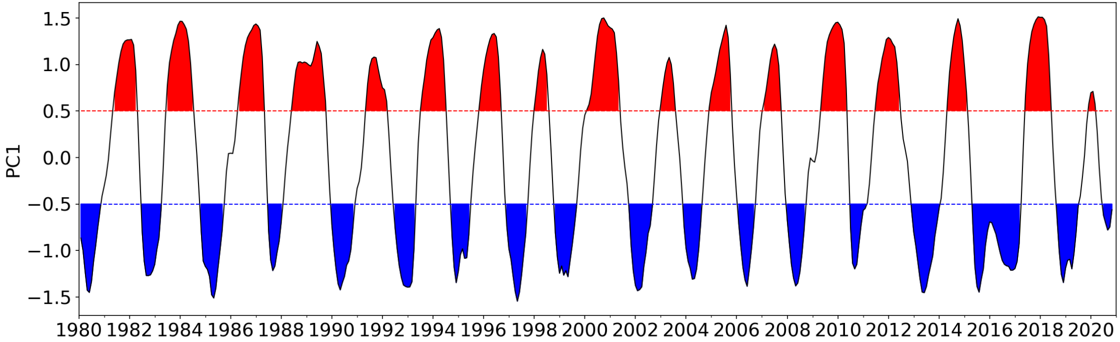

(b) EOF PC2

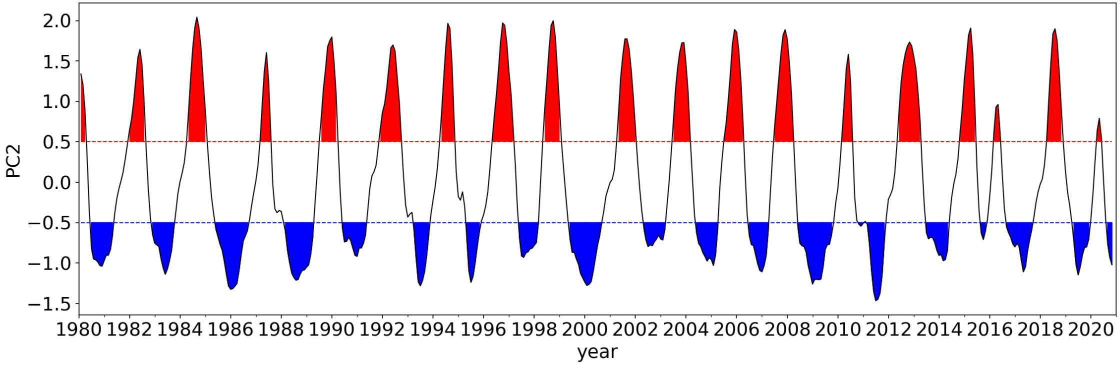

Figure 1. Time series of the first two principal components (PCs) of QBO from 1979 to 2020 obtained by an EOF analysis applied to the FUB QBO data from 70 to 10 hPa. **(a)** PC1, indicating the QBO phase in the middle stratosphere at 20 hPa. **(b)** PC2, indicating the QBO phase in the lower stratosphere at 50 hPa. Red/blue colours are shaded where the QBO indexes are greater/less than half of its standard deviation, indicating the QBOW/QBOE phases.

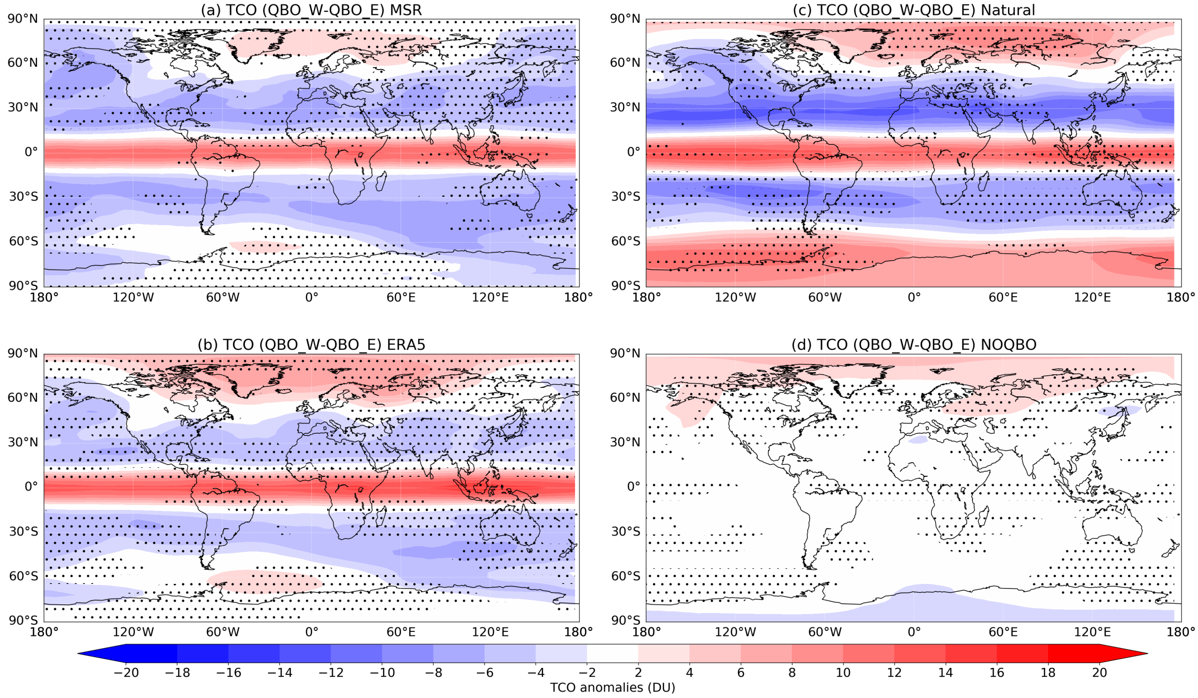

Figure 2. Influences of QBO (QBOW-QBOE) on global total column ozone (TCO) based on monthly anomalies from different data sets. **(a)** MSR2 data 1979-2020. **(b)** ERA5 data 1979-2020. **(c)** CESM-WACCM Natural run 1979-2020. **(d)** CESM-WACCM NOQBO run 1979-2020. Stippled areas indicate results that are statistically significant over the 90% level, using the two-tailed Student's t-test.

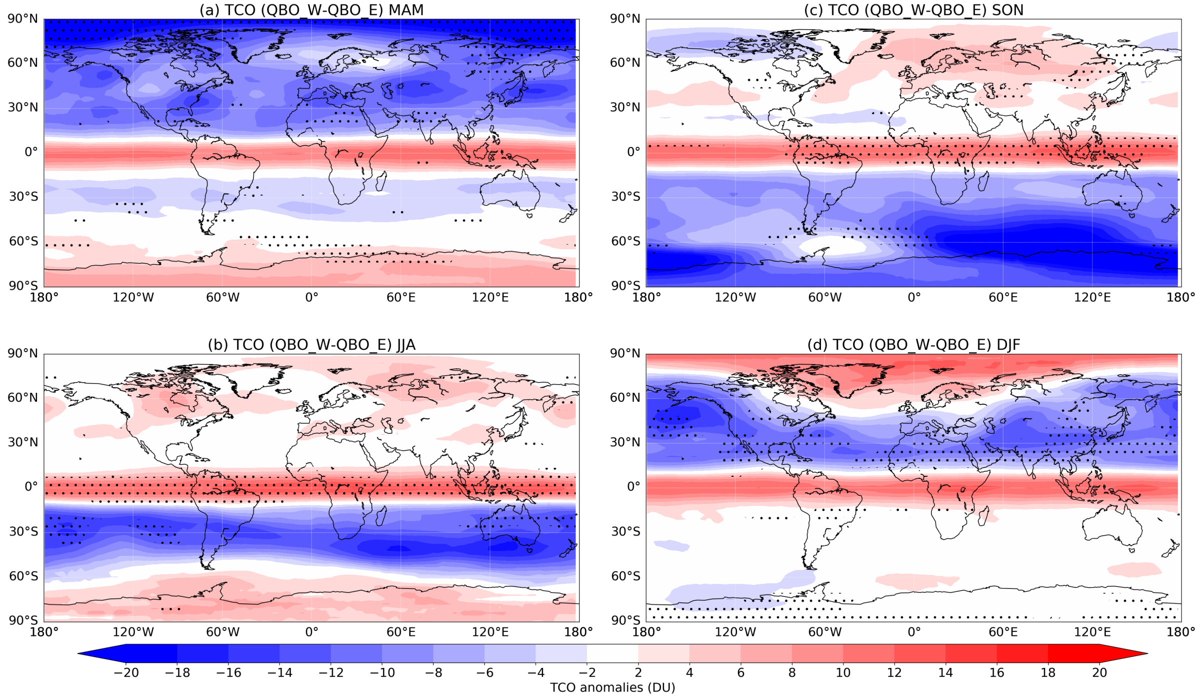

Figure 3. Influences of QBO (QBOW-QBOE) on global total column ozone (TCO) in different seasons based on MSR2 data 1979-2020. **(a)** MAM. **(b)** JJA. **(c)** SON. **(d)** DJF. Stippled areas indicate results that are statistically significant over the 90% level, using the two-tailed Student's t-test.

https://doi.org/10.5194/acp-2022-174
Preprint. Discussion started: 29 March 2022

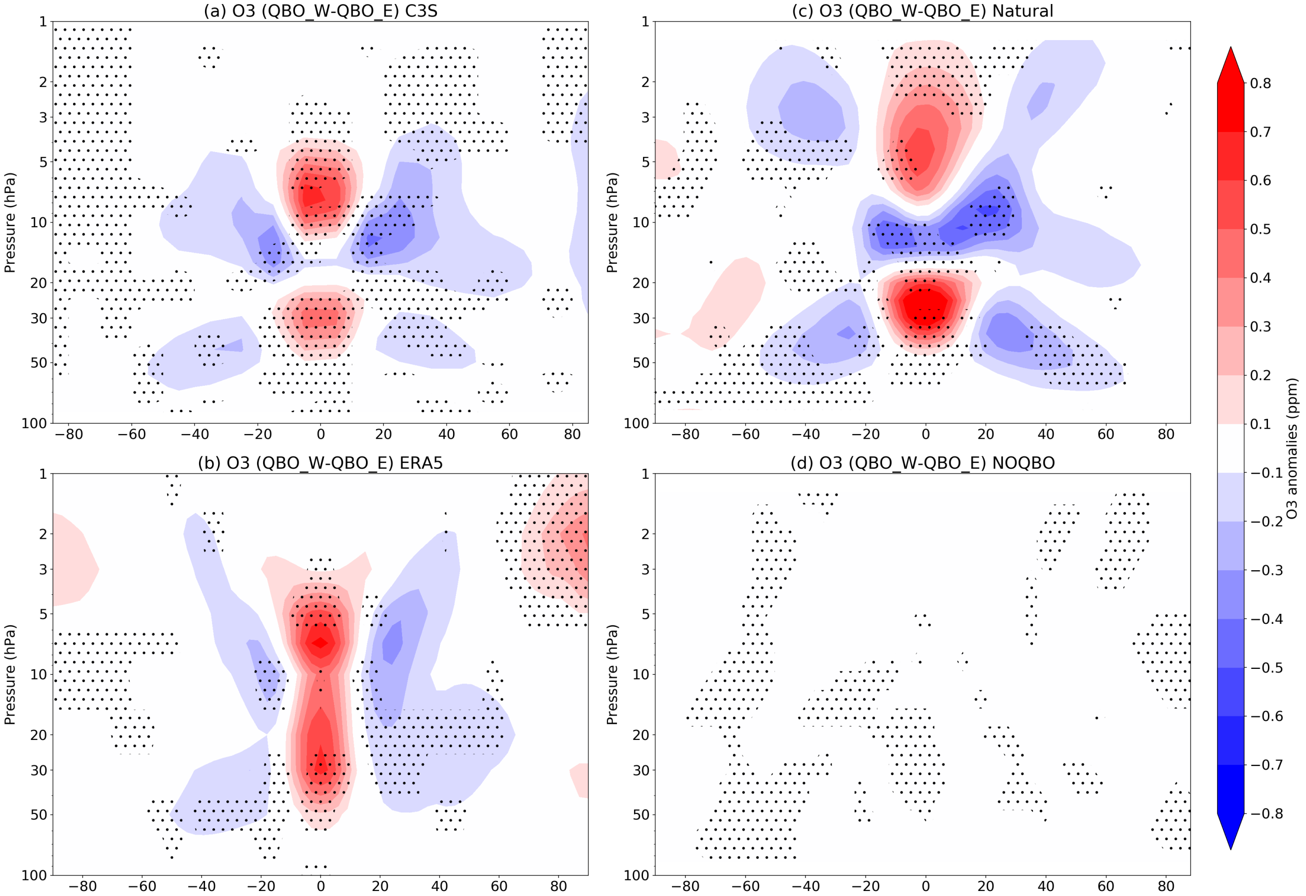

Figure 4. Latitude-height cross-section of ozone anomalies associated with QBO (QBOW-QBOE) based on monthly anomalies of zonal mean ozone from different data sets for the period 1985-2020. **(a)** Merged satellite data from C3S. **(b)** ERA5 data. **(c)** CESM-WACCM Natural run. **(d)** CESM-WACCM NOQBO run. Stippled areas indicate results that are statistically significant over the 90% level, using the two-tailed Student's t-test.

https://doi.org/10.5194/acp-2022-174
Preprint. Discussion started: 29 March 2022

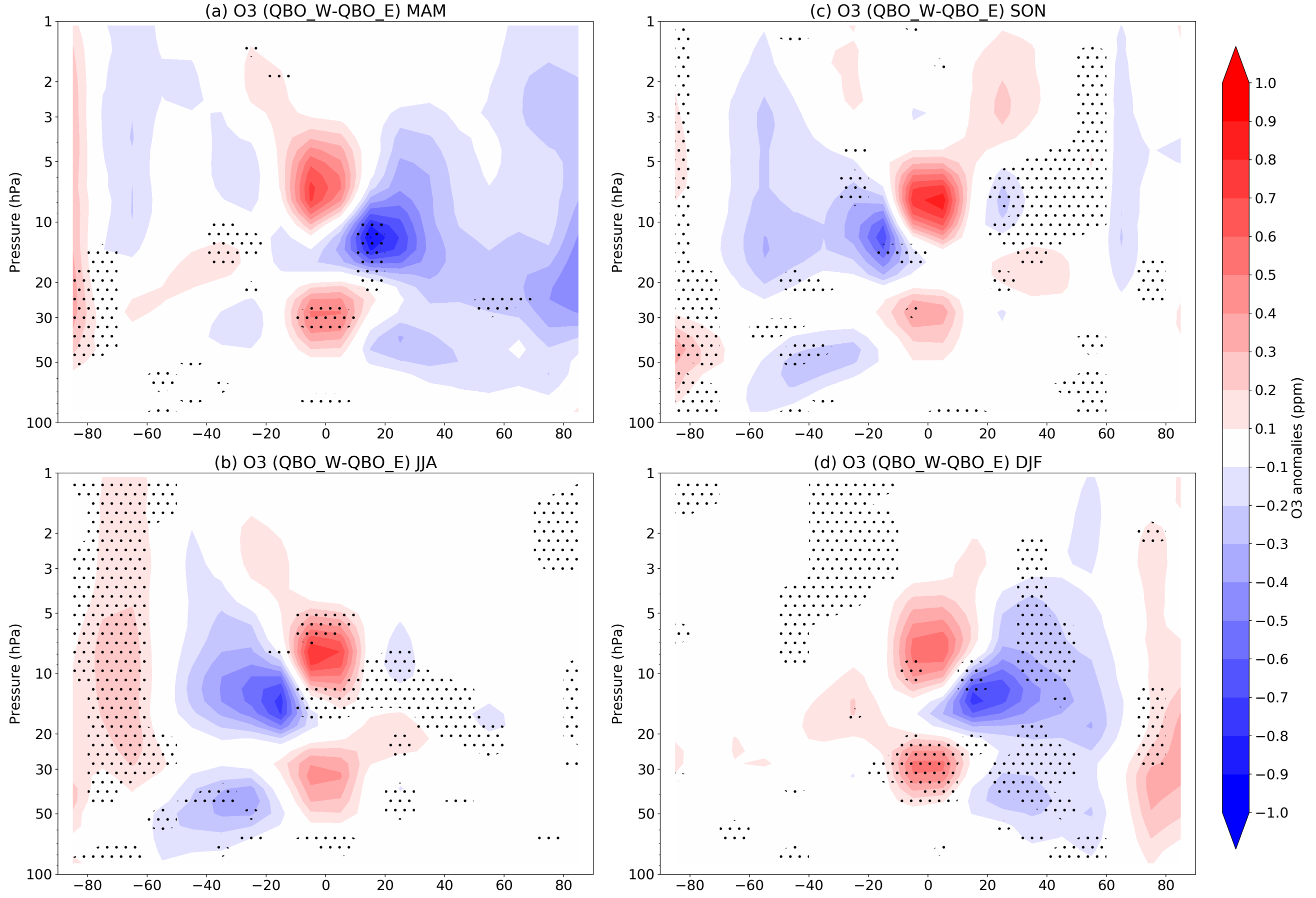

Figure 5. Latitude-height cross-section of ozone anomalies associated with QBO (QBOW-QBOE) based on merged satellite data from C3S for the period 1985-2020. **(a)** MAM. **(b)** JJA. **(c)** SON. **(d)** DJF. Stippled areas indicate results that are statistically significant over the 90% level, using the two-tailed Student's t-test.

https://doi.org/10.5194/acp-2022-174
Preprint. Discussion started: 29 March 2022

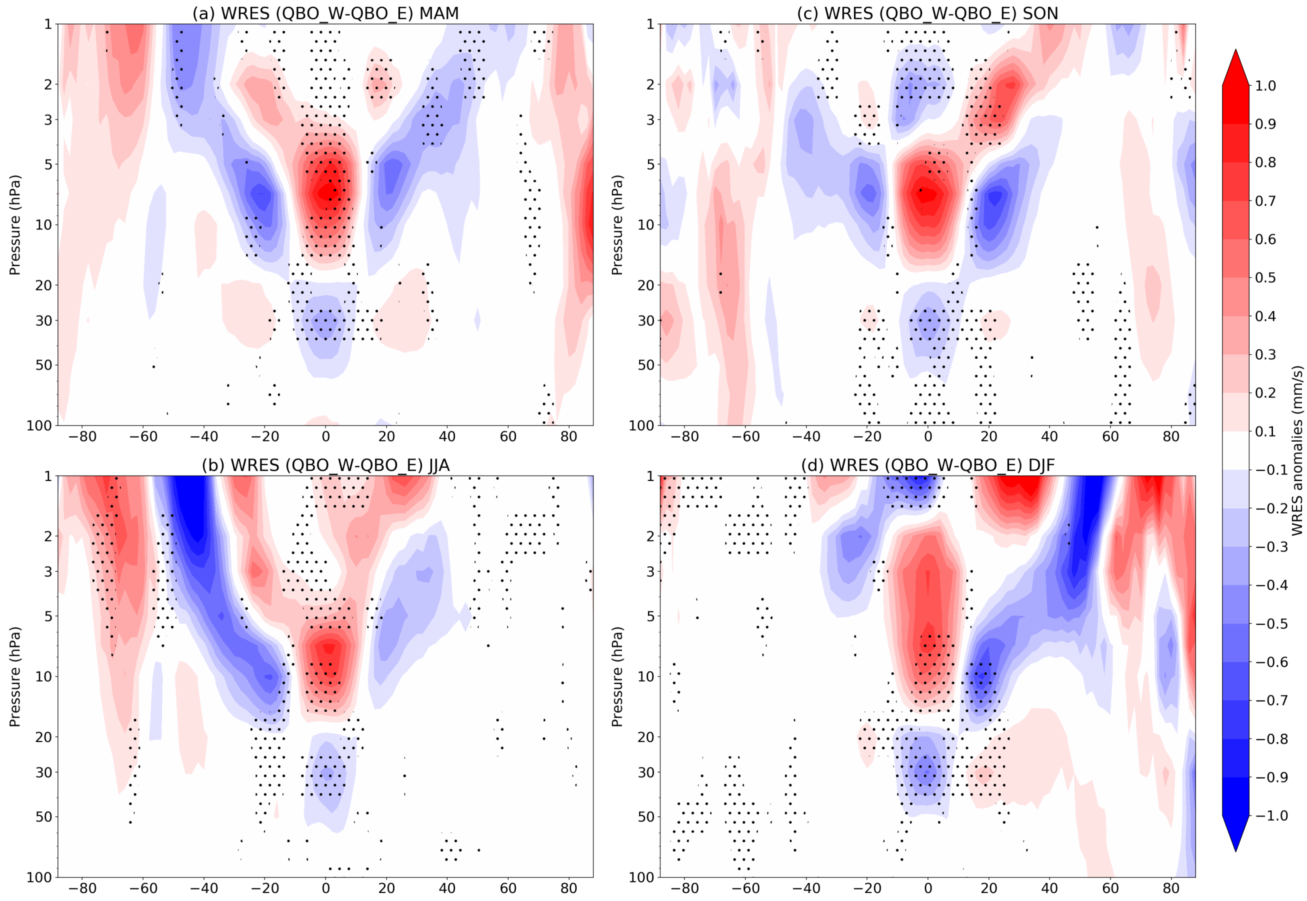

Figure 6. Latitude-height cross-section of w* (vertical component of the BDC) anomalies associated with QBO (QBOW-QBOE) from ERA5 data for the period 1985-2020. **(a)** MAM. **(b)** JJA. **(c)** SON. **(d)** DJF. Stippled areas indicate results that are statistically significant over the 90% level, using the two-tailed Student's t-test.

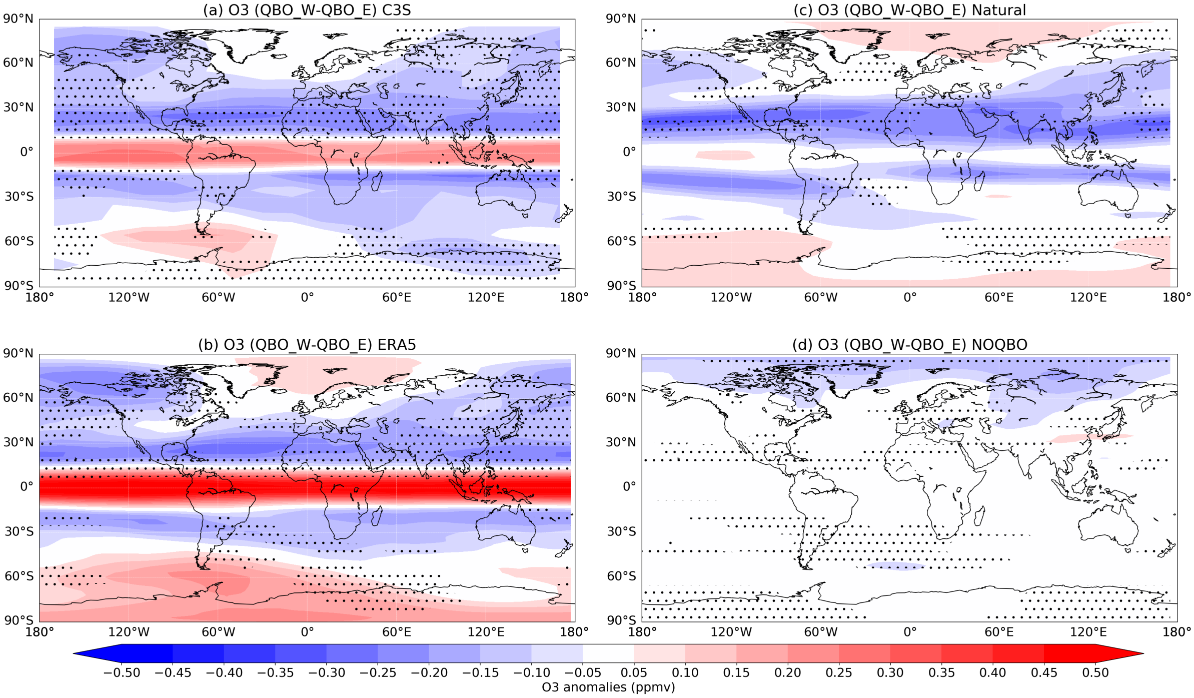

Figure 7. Influences of QBO (QBOW-QBOE) on global stratospheric ozone (10 hPa) based on monthly anomalies from different data sets for the period 2002-2020. **(a)** Merged satellite data from C3S. **(b)** ERA5 data. **(c)** CESM-WACCM Natural run. **(d)** CESM-WACCM NOQBO run. Stippled areas indicate results that are statistically significant over the 90% level, using the two-tailed Student's t-test.

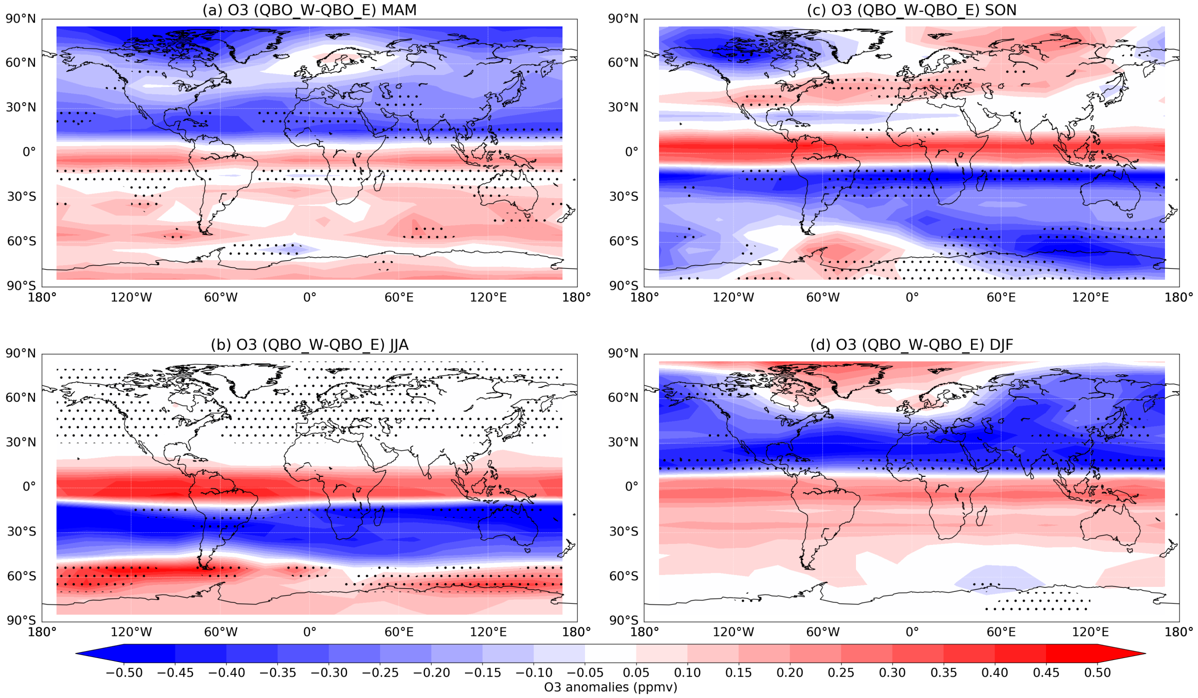

Figure 8. Influences of QBO (QBOW-QBOE) on global stratospheric ozone (10 hPa) based on merged satellite data from C3S for the period 2002-2020. **(a)** MAM. **(b)** JJA. **(c)** SON. **(d)** DJF. Stippled areas indicate results that are statistically significant over the 90% level, using the two-tailed Student's t-test.

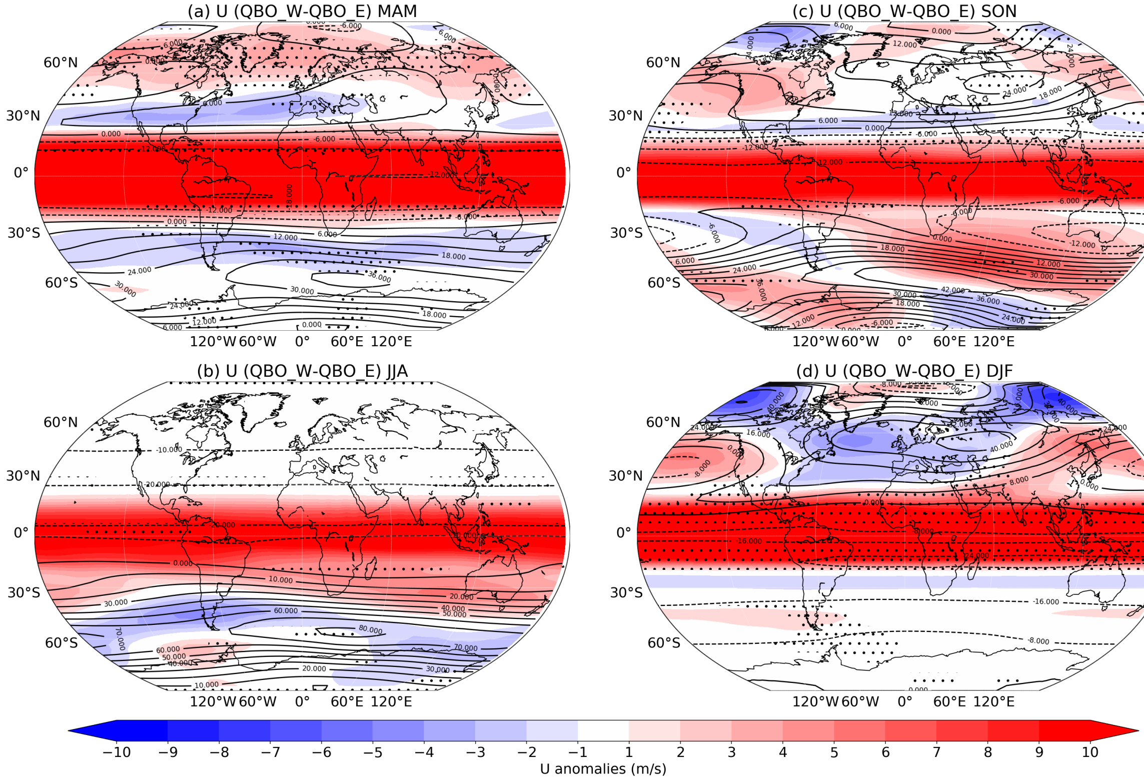

Figure 9. Influences of QBO (QBOW-QBOE) on the global zonal wind (U at 10 hPa) based on ERA5 data for the period 1979-2020. The climatological values of zonal winds in each season are also shown (contour lines). **(a)** MAM. **(b)** JJA. **(c)** SON. **(d)** DJF. Stippled areas indicate results that are statistically significant over the 90% level, using the two-tailed Student's t-test.

https://doi.org/10.5194/acp-2022-174
Preprint. Discussion started: 29 March 2022

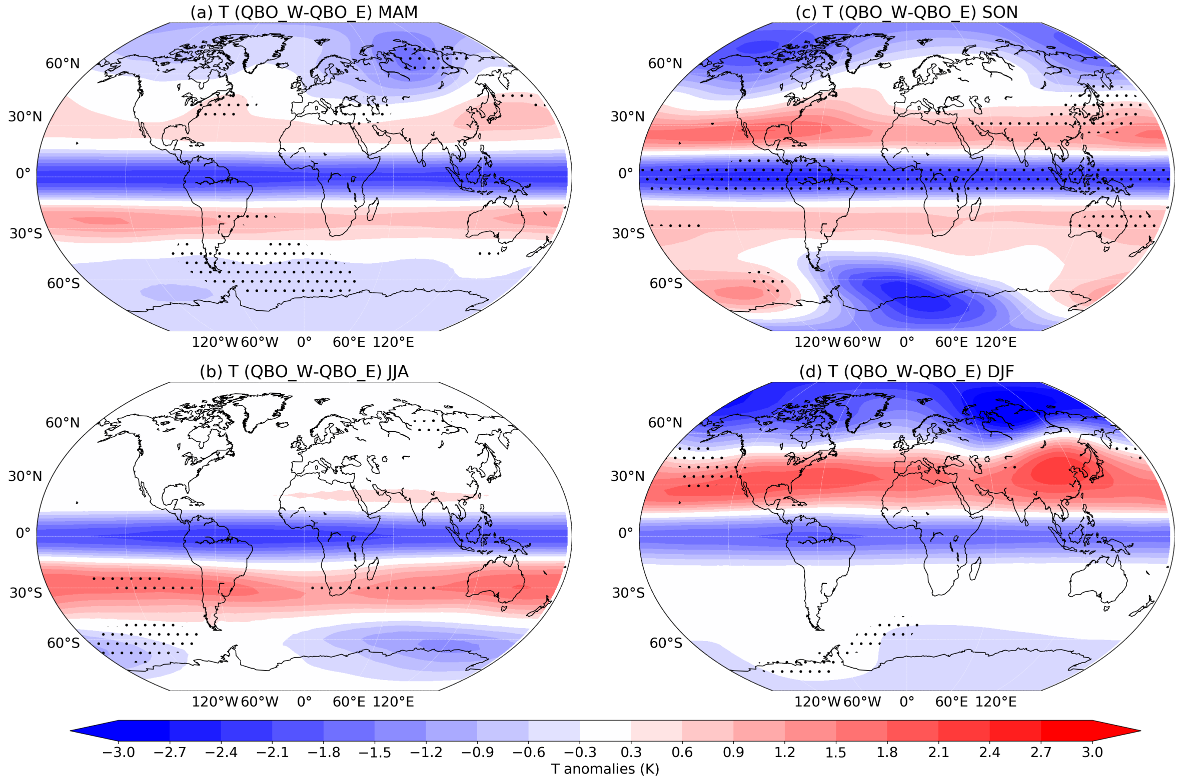

Figure 10. Influences of QBO (QBOW-QBOE) on global temperature (T at 10 hPa) based on ERA5 data for the period 1979-2020. The climatological values of temperature in each season are also shown (contour lines). **(a)** MAM. **(b)** JJA. **(c)** SON. **(d)** DJF. Stippled areas indicate results that are statistically significant over the 90% level, using the two-tailed Student's t-test.

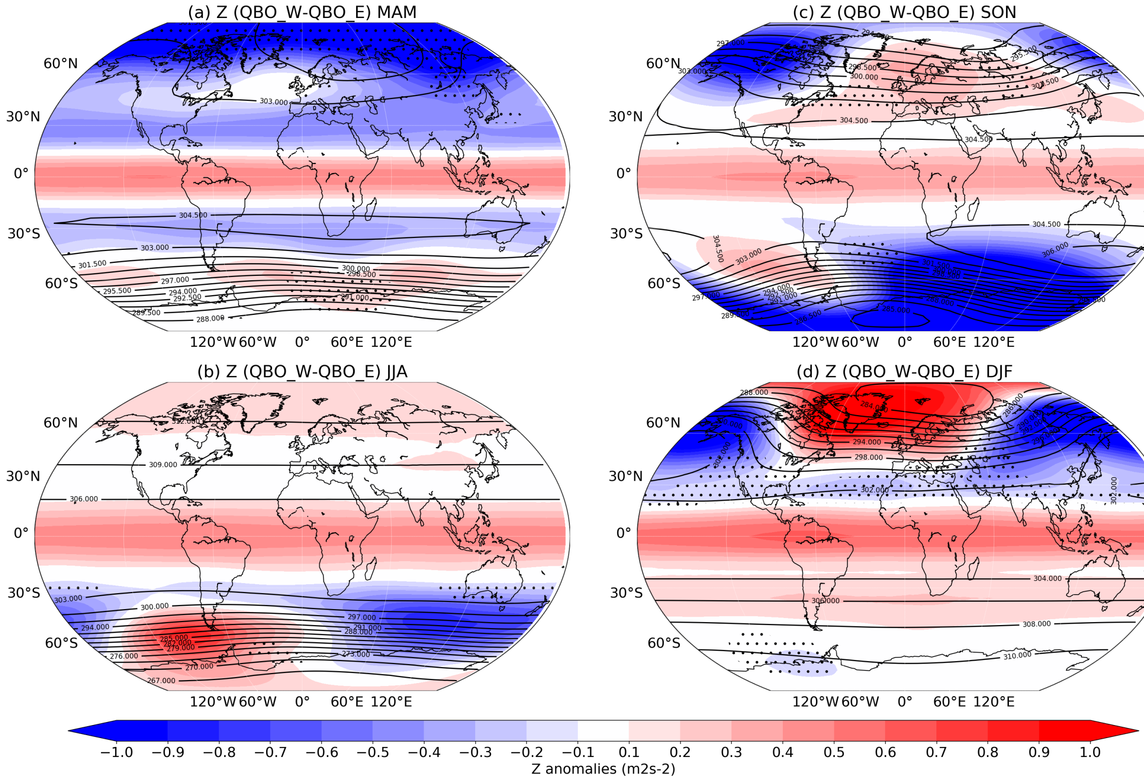

Figure 11. Influences of QBO (QBOW-QBOE) on global geopotential height (Z at 10 hPa) based on ERA5 data for the period 1979-2020. The climatological values of geopotential height in each season are also shown (contour lines). **(a)** MAM. **(b)** JJA. **(c)** SON. **(d)** DJF. Stippled areas indicate results that are statistically significant over the 90% level, using the two-tailed Student's t-test.

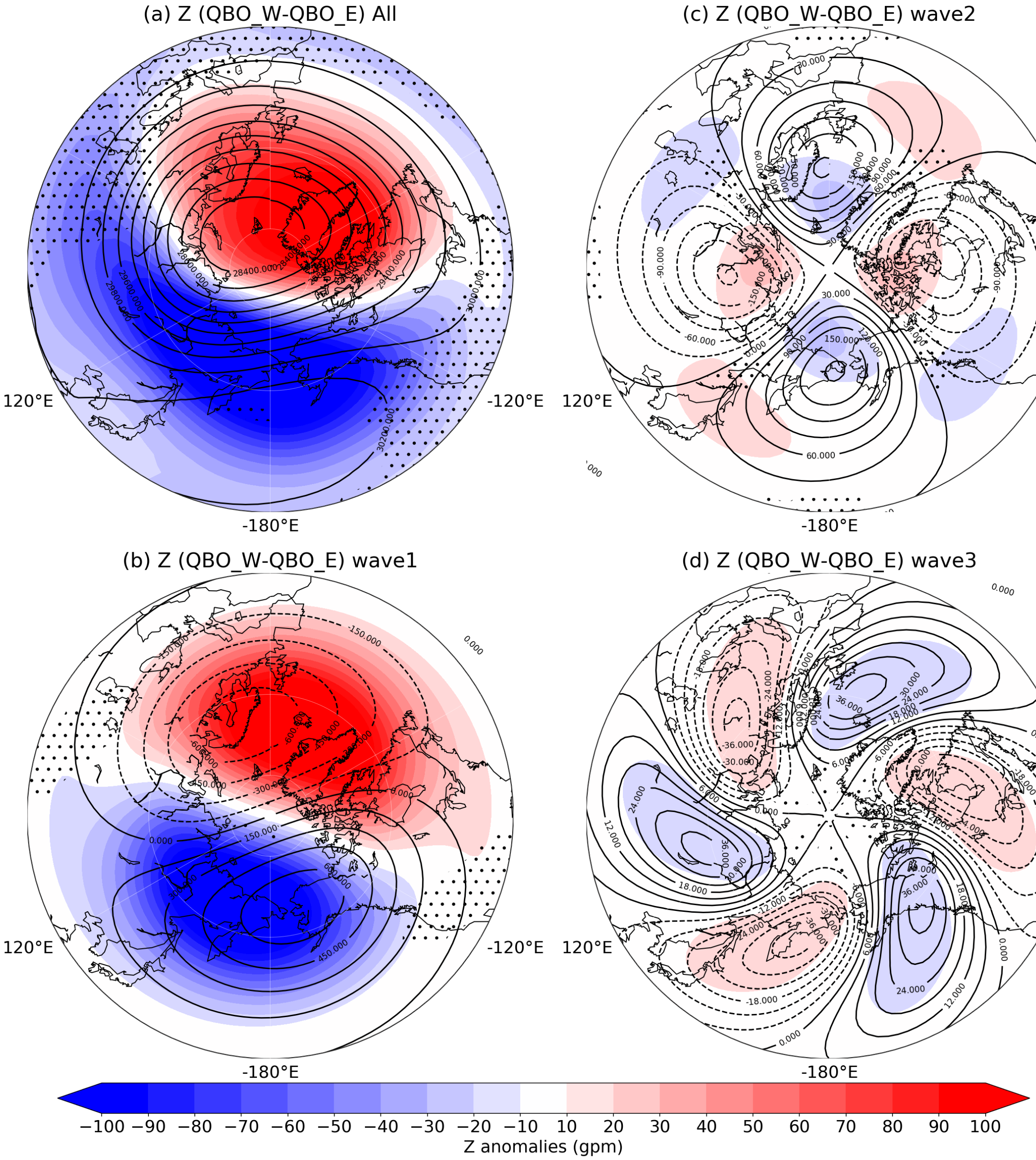

Figure 12. (a) Influences of QBO (QBOW-QBOE) on geopotential height (Z at 10 hPa) in the northern hemisphere winter (DJF) based on ERA5 data for the period 1979-2020. **(b-d)** The corresponding changes of geopotential height associated with QBO in wave numbers 1-3. The climatological values of geopotential height in winter as well as the climatological patterns of wave numbers 1-3 are also shown (contour lines). Stippled areas indicate results that are statistically significant over the 90% level, using the two-tailed Student's t-test.